[22] Schrade, H., Bez, W., Höcker, K. H., and Kaeppeler, H. J., "Zur Theorie der Ohmschen Heizung vollionisierter Plasman," *Zeitschrift für Naturforschung*, Vol. 15a, No. 2, 1960, pp. 155–168.

[23] Weizel, W. and Rompe, R., "Tragerbeweglichkeit und Leitfahigkeit," *Theorie elektrischer Lightbogen und Funken*, Leipzig, 1949, pp. 10–13.

[24] Fay, J. A., "Comments on Convective Flexure of a Plasma Conductor," *The Physics of Fluids*, Vol. 7, No. 4, April 1967, pp. 621–622.

[25] Schlichling, H. and Truckenbrodt, E., "Zwei und dreidimensionale Strömungen," *Aerodynamik des Flugzeuges*, Vol. 1, Springer, 1959, pp. 61–63.

[26] Bose, T. K., Noel, M. B., and Massier, P. F., "Comparison of Theoretical and Experimental Deflection of a Blown Arc," *JPL Space Programs Summary* 37–61, Vol. III, Feb. 1970, pp. 242–246.

[27] Benenson, D. M., Baker, A. J., and Cenker, A. A., jr., "Diagnostics on Steady State Cross-flow Arcs," Rept. ARL-68-0109, May 1968, Aerospace Research Labs., Wright-Patterson Air Force Base, Ohio; also *Transactions of the ASME, Ser. C: Journal of Heat Transfer*, Vol. 92, No. 2, May 1970, pp. 276–284.

JANUARY 1972 AIAA JOURNAL VOL. 10, NO. 1

Anode Phenomena in High-Current Accelerators

RONALD C. OBERTH* AND ROBERT G. JAHN†
Princeton University, Princeton, N.J.

Experimental study of various anode processes in quasi-steady magnetoplasmadynamic accelerators has clarified certain aspects of the current conduction and power loss mechanisms in these devices. Measurements of local anode-fall voltage and anode current density in argon arcs operated at currents of 8.7, 17.5, and 42.0 ka indicate an inverse relationship between these two quantities which translates into a significant decrease in fractional anode power loss for operation in the megawatt range of pulse power. For matched and overfed mass flows, anode current conduction appears to be accomplished by random thermal flux of electrons from the adjacent arc plasma. For underfed conditions, substantial electric fields develop around the anode to enhance anode current conduction from the lower plasma density environment. Approximate calculations indicate that these fields accomplish this by a combination of tensor electron conduction and additional ionization through local resistive heating.

I. Background

THE investigation of anode phenomena in high-current plasma accelerators is motivated by the well-known, yet poorly understood, severe anode power losses which plague these devices. Experimental studies on steady, low-power magnetoplasmadynamic (MPD) arc indicate that from 30%–60% of the total input power may be lost at the anode, but also suggest a tendency towards lower fractional anode power loss with increasing arc power.[1,2] Effective exploitation of the latter effect has been hindered by the magnitude of the heat transfer and by the intolerable power demands which accompany steady MPD arc operation beyond the kw power range, but it now seems possible to achieve this reduction in relative anode power loss, and the corresponding increase in thermal efficiency, through high-power, quasi-steady arc operation.[3,4]

Briefly, quasi-steady plasma acceleration involves the operation of self-field electromagnetic thrusters in repetitive high-power pulses of sufficient duration that essentially steady acceleration processes of high thermal efficiency prevail over most of the pulse, but at repetition rates commensurate with available space power supplies and reasonable heat rejection capabilities. This concept also affords the opportunity for variable thrust and mean power consumption, without compromise in specific impulse or thruster efficiency, via simple duty-cycle adjustment.

The quasi-steady MPD device employed in the present study of anode power loss and anode current conduction closely replicates the conventional steady MPD arc configuration, but on a scale one order of magnitude larger to permit detailed interior diagnostics. A schematic diagram and photograph of this apparatus are shown in Figs. 1 and 2. Briefly,[3] it consists of a cylindrical discharge chamber with a $\frac{3}{4}$-in.-diam conical tungsten cathode and a $7\frac{1}{2}$-in.-diam aluminum anode with a 4-in.-diam orifice. It is powered by a 130μf × 10 kv capacitor line which

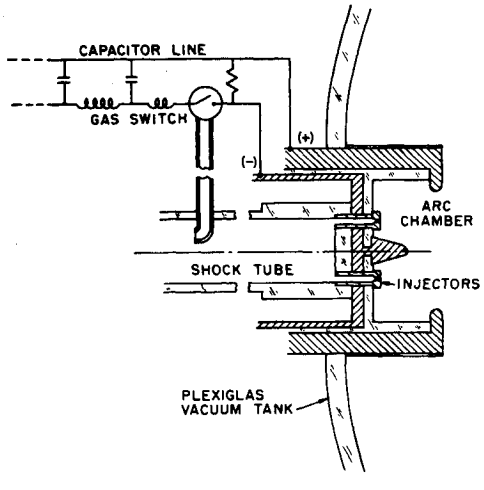

Fig. 1 Accelerator schematic.

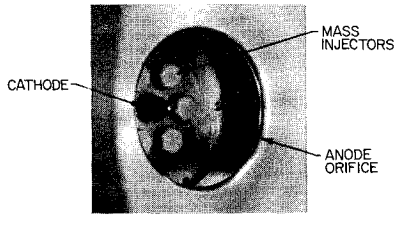

Fig. 2 Accelerator chamber.

Presented as Paper 71-198 at the AIAA 9th Aerospace Sciences Meeting, New York, January 25–27, 1971; submitted February 16, 1971; revision received September 15, 1971. This work supported by NASA NGL 31-001-005.

Index categories: Electric and Advanced Space Propulsion: Plasma Dynamics and MHD.

* Graduate Student, Guggenheim Aerospace Propulsion Laboratories; presently at Elektrophysikaliches Institut, Technische Universität, München, West Germany.

† Dean of Engineering and Applied Science. Associate Fellow AIAA.

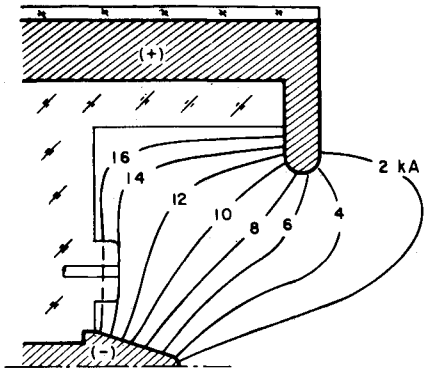

Fig. 3 Quasi-steady current distribution; $J = 17.5$ ka, $\dot{m} = 5.9$ g/sec.

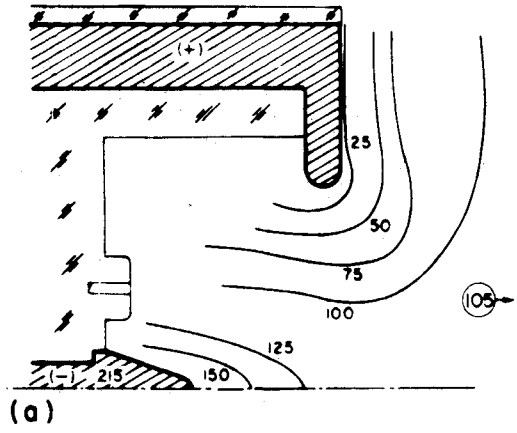

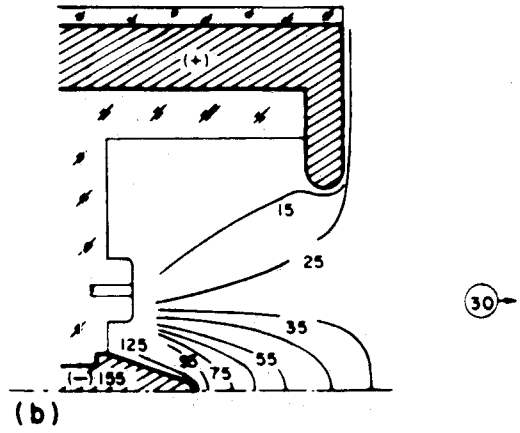

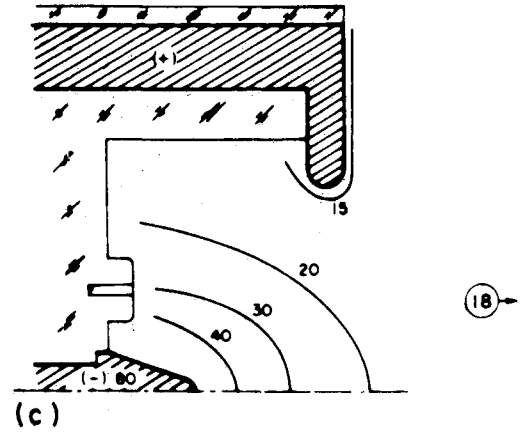

Fig. 4 Equipotential profiles at 17.5 ka: a) $\dot{m} = 1.2$ g/sec; b) $\dot{m} = 5.9$ g/sec; c) $\dot{m} = 36$ g/sec.

can provide rectangular current pulses ranging from 4 ka × 600 μsec to 140 ka × 20 μsec. Propellant gas is injected at selected rates through six calibrated orifices in the arc chamber end plate from a high-pressure reservoir abruptly established by the end wall stagnation of the flow in a simple shock tube. An adjustable bleed line from the same shock tube triggers the discharge current switch, thereby controlling the correlation of the mass flow pattern with the arc current profile.

Earlier studies on this device[5,6] established the main features of the current density distribution and plasma potential patterns at various combinations of arc current and argon mass flow rate. For example, Fig. 3 shows the distribution of current density in the arc chamber and along the anode surface at an arc current of 17.5 ka and mass flow rate of 5.9 g/sec, which is a matched operating condition.[5,6] These current contours indicate that most of the arc current concentrates on the upstream lip of the anode in preference to other portions of the anode surface. Figure 4 displays floating potential contours for the same matched conditions, as well as for operation at an underfed mass flow of 1.2 g/sec, and an overfed flow of 36.0 g/sec. The most obvious aspect of these patterns is that the major portion of the arc power is deposited in the cathode region of the arc, implying that this region of high current density and high electric field is primarily responsible for the high plasma velocities observed downstream.[6] With regard to the anode regions, these patterns display the magnitude of the normal anode fall, and show the importance of matching the mass flow rate to the total arc current. Figure 4b, for the matched mass flow of 5.9 g/sec, displays an anode fall of less than 15 v over the upstream lip of the anode where current density is a maximum, and somewhat higher values on the downstream face where current density is lower. The dependence of anode fall voltage on local anode current density and its implication for anode power losses are discussed in Secs. II and III.

A similar anode fall is seen in the overfed case, Fig. 4c. In the underfed case, Fig. 4a, however, a substantially larger and broader electric field appears adjacent to the anode surface, suggesting the onset of anode conduction difficulties at this operating condition. The relation of the mass flow rate to the field development and conduction processes in the anode region is examined in Sec. IV.

II. Anode Fall Measurements

In order to explore further the dependence of anode fall voltage on local anode current density, a series of detailed electrostatic and magnetic probe measurements have been taken over the anode surface during quasi-steady arc operation at three different matched conditions, 8.7 ka × 1.2 g/sec, 17.5 ka × 5.9 g/sec, and 42.0 ka × 36.0 g/sec, where the arc behavior is well-defined and reproducible. The anode falls are determined from floating potential measurements taken adjacent to the surface with electrostatic probes whose exposed elements are $\frac{1}{16}$-in.-diam hemispheres. Some of these are inserted axially upstream into the discharge and bent to allow access to the regions behind the anode lip; the front face of the anode is monitored by radially inserted probes. All leads to the probe sensing surfaces are coaxially shielded, and the signals are presented to the oscilloscope via a Tektronix Model 6013A voltage probe of 10^8 ohm impedance. Simultaneously with the collection of floating potential data, the magnetic field values over the anode surface are measured by magnetic induction coils, 100 turns of No. 40 Formvar wire on $\frac{3}{32}$-in.-diam nylon spools, which are also mounted on bent shafts to permit access to the back anode region. From the measured values of magnetic field at these locations, the anode current density distribution is readily deduced.[7]

In the present context, anode fall refers to the voltage difference between the anode surface and a point in the plasma about 0.1 cm off of the surface. The measured values of floating potential must be corrected to plasma potentials before the true anode falls can be assigned. For an argon plasma in which ion

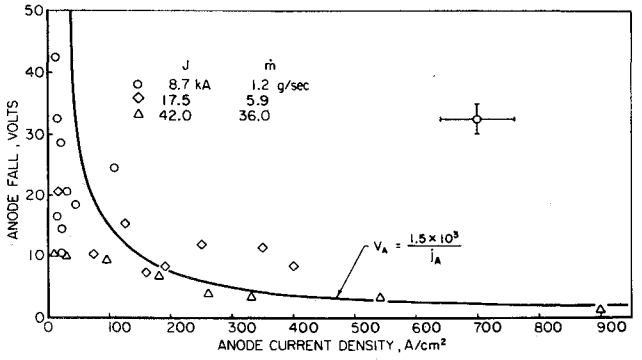

Fig. 5 Anode fall variation with local current density.

streaming velocities are negligible—a good assumption for most of the region adjacent to the anode surface—the difference between floating and plasma potential is given by[8]

$$V_p - V_f = (kT_e/e)[\ln(m_i/m_e)^{1/2}] \approx 5.6\,kT_e/e \qquad (1)$$

where T_e is taken to be 1.5 ev, based on several other studies (see Sec. IV), so that floating potential measurements should be adjusted some 8.4 v closer to anode potential.

A composite graph of anode fall vs corresponding local anode current density for the three matched operating conditions is shown in Fig. 5. The indicated inverse dependence of anode fall on local anode current density can be reasonably approximated by the reciprocal fit, $V_a = 1.5\times10^3/j_a$, which in turn implies a constant anode power density, $P_a = j_a V_a = 1500$ w/cm^2. Regardless of its precise form, this inverse dependence clearly has major implications for the over-all efficiency of high-power accelerators of this type.

The anode fall data appear to agree qualitatively with the classical anode fall theories of Bez and Höcker.[9,10] Their model is based on the assumption that the major function of the anode fall is the production of ions, and that this is accomplished by either of two mechanisms: field ionization or thermal ionization. Field ionization involves collisional ionization by electrons that have been directly accelerated by the anode fall field; the anode fall voltage is therefore greater than the ionization potential of the operating gas and the anode current densities are generally low, say less than about 50 amp/cm^2. Thermal ionization, on the other hand, involves ionization by electrons whose motion has become thermalized in the fall zone by elastic collisions. Since only the high-energy electrons in the distribution need engage in ionizing collisions, the anode fall can now be lower than the ionization potential of the gas, but much higher anode current densities may be accommodated. In this spirit, the anode fall data of Fig. 5 may reflect a transition from field ionization at low-anode current densities to thermal ionization at high-anode current densities with a corresponding decrease in anode fall voltage.[11]

III. Anode Power Loss

The total power loss at the anode of a high-current arc discharge may be written[1]

$$P_a = P_{ca} + P_{ra} + \int j_a[(\tfrac{5}{2}kT_e/e) + V_a + \phi_a]\,dA \qquad (2)$$

where P_{ca} and P_{ra} are the convective and radiative contributions, and the integral is taken over the anode surface, and represents the heat transfer implicit in the electron current to it. Here T_e is the electron temperature of the adjacent plasma, V_a denotes the anode fall, and ϕ_a is the work function of the anode metal. The term $\frac{5}{2}(j_a kT_e/e)$ accounts for the transport of electron thermal energy from the plasma.

Recent experiments employing a semiconductor photo diode have indicated that only a few percent of the total input power is radiated from the arc plasma.[12] Since only a small fraction of this radiation is intercepted by the anode surface, the radiative term, P_{ra}, may be neglected for the present. Similarly, convective heat transfer from the streaming plasma to the anode surface is assumed to be most significant at the lip region of the anode, where it may be evaluated by compressible boundary layer methods.[13] Using generous estimates for all parameters, the value of P_{ca} is computed to be about 20 kw. This is less than 1% of the total input power for matched quasi-steady arc operation at 17.5 ka, hence is also neglected.

There remains only the integral term representing energy carried to the anode by conduction electrons. Since T_e and ϕ_a are essentially constant over most of the anode surface, this may be rewritten

$$P_a = J(\tfrac{5}{2}kT_e/e + \phi_a) + \int j_a V_a\,dA \qquad (3)$$

where J is the total arc current. For operation at the three matched conditions cited earlier, the empirical relation, $V_a = 1.5\times10^3/j_a$ (w/amp/cm^2), can be used to evaluate the integral. Taking approximate values of T_e and ϕ_a of 1.5 ev and 3.5 v, respectively, and an anode surface area of 300 cm^2, the anode power becomes

$$P_a \approx 7.25\,J + 450 \quad \text{(kw)} \qquad (4)$$

for J in ka.

Since the arc current increases less than linearly with total arc power, it is clear that fractional anode power loss decreases substantially with arc power. This result is displayed in Fig. 6

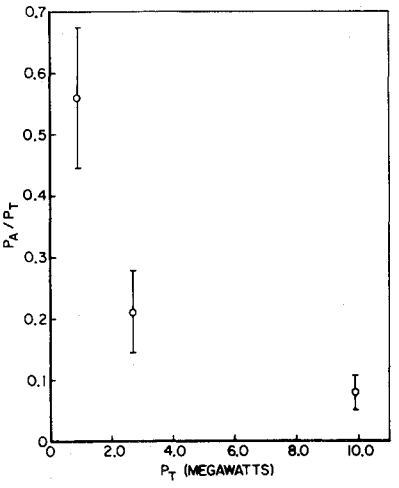

Fig. 6 Fractional anode power variation with total arc power at matched conditions.

which plots the fractional anode power loss for the three matched conditions against the total input arc power P_t. Observe that P_a/P_t decreases from over 50% to less than 10% for an increase in arc power from 1.5 to 10 Mw. It follows that correspondingly higher thermal efficiencies should prevail for the higher power operation.

IV. Anode Current Conduction

Electron Temperature and Density Measurements

Models of the mechanisms of current conduction to the anode surface ultimately rest on the values of electron density and temperature prevailing in the adjacent plasma. To accumulate this information, a series of double Langmuir probe measurements have been carried out at various locations in the quasi-steady MPD discharge. Briefly,[14,15] these probes consist of two separately shielded and biased $\frac{1}{8}$-in. long exposed tips of 3-mil tungsten wire oriented parallel to the flow axis to minimize streaming effects, and mounted on the same support tube to sample essentially the same plasma. A schematic of the probe and circuitry is shown in Fig. 7. The probe radius is considerably less than the anticipated electron-ion mean free-paths and

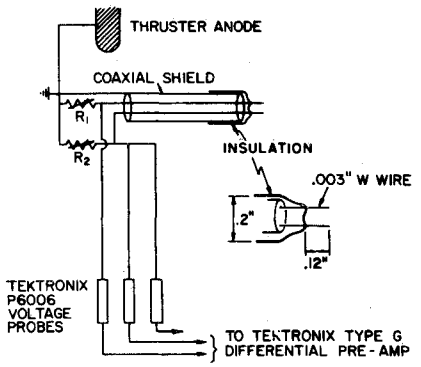

Fig. 7 Schematic of twin Langmuir probe.

electron gyro radii in the anode region of the arc, thus reducing the influence of collisional and magnetic field effects on probe behavior, but it is substantially larger than the local Debye length, thereby removing the influence of sheath size on the electron saturation current drawn by the probe. One of the probes is mounted on a bent support shaft to allow access to the back portion of the anode. The probe voltages developed across different resistor pairs are monitored with Tektronix P6006 voltage probes and displayed on an oscilloscope. The electron temperature is obtained from the ratio of the two probe tip currents, J_1 and J_2, and the difference in probe voltages, ΔV_{12}, provided both tips operate on the electron-retarding branch of the probe characteristic where the ion current to the probe can be neglected, in which case,

$$kT_e = e\Delta V_{12}/\ln(J_1/J_2) \tag{5}$$

Electron number density is determined somewhat less precisely by ascertaining when one of the probe tips begins to draw electron saturation current and thus is at the local plasma potential, as evidenced by a sudden increase in the values of kT_e computed via the aforementioned relation. From the measured current to the probe tip at this condition, and from the previously determined electron temperature, the local electron number density is extracted from the relation.

$$J_p^* = n_e e A_p (kT_e/2\pi m_e)^{1/2} \tag{6}$$

where A_p is the probe surface area and m_e the electron mass. Figure 8 displays typical results of such electron temperature and density measurements.

The observed plasma potential and current density patterns in the vicinity of the anode surface also provide useful hints in the formulation of anode current conduction models. Recall the previous measurements with floating electrostatic probes which revealed that substantial electric fields develop in the anode region for operation below the matched mass flow for a given arc current (Fig. 4a), while at matched or overfed mass flows all fields were confined to the cathode region of the discharge except for a narrow sheath drop adjacent to the anode surface (Figs. 4b, c). Figure 9 superimposes on plots of plasma potential contours, determined from floating potential data by the method outlined in Sec. II, the corresponding current contours for quasi-steady operation at mass flows of 1.2 g/sec, 5.9 g/sec, 36.0 g/sec, and a common current of 17.5 ka. In addition to the previously observed electric field growth around the anode for the 1.2 g/sec case (Fig. 9a), it is also apparent that a greater portion of the anode surface participates in the current conduction at this underfed situation.

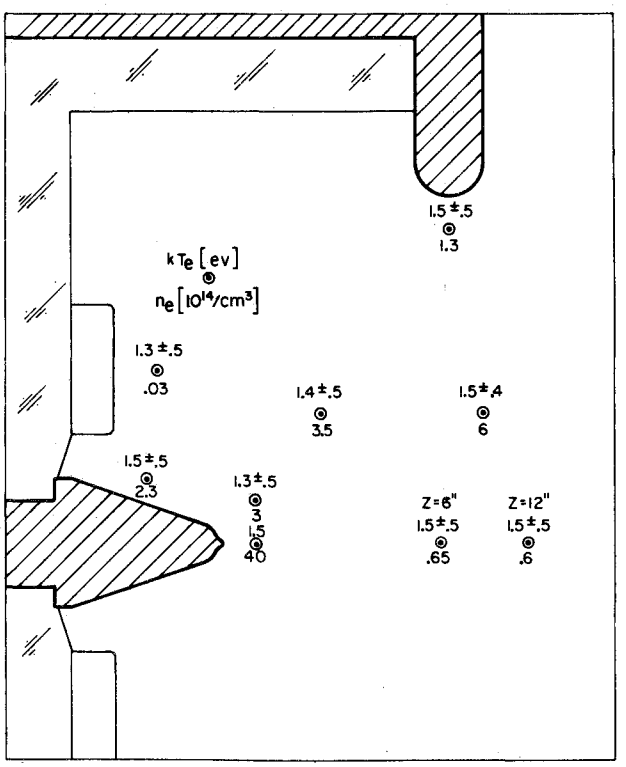

Fig. 8 Typical electron temperature and number densities; $J = 17.5$ ka, $\dot{m} = 5.9$ g/sec.

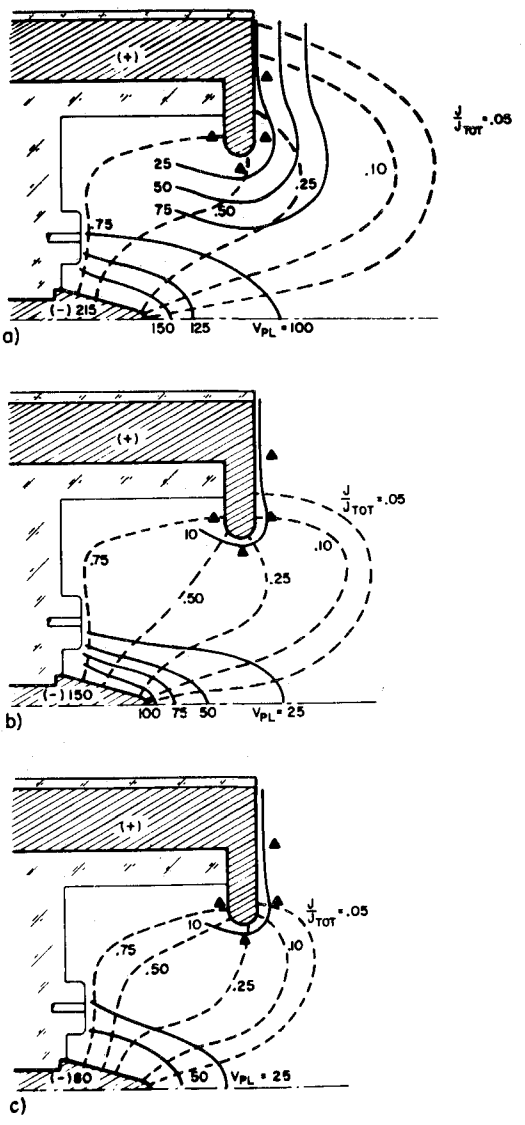

Fig. 9 Plasma potential and enclosed current contours at 17.5 ka: a) $\dot{m} = 1.2$ g/sec; b) $\dot{m} = 5.9$ g/sec; c) $\dot{m} = 36$ g/sec.

Anode Current Conduction by Random Electron Flux

In matched and overfed operation of the arc, where there is negligible electric field in the plasma adjacent to the anode fall, it must be presumed that the required anode current enters the fall region via thermal electron diffusion from the equipotential plasma. This can be verified by an elementary calculaton based on the observed electron temperatures and densities in that region. Assuming a Maxwell-Boltzmann distribution for the electrons near the plasma boundary, the electron current density at this location due to random flux is simply related to the electron mean thermal speed, $c_e = (8kT_e/\pi m_e)^{1/2}$

$$j_e = en_e c_e/4 = en_e(kT_e/2\pi m_e)^{1/2} \tag{7}$$

Figures 10a, b compare this random flux current density, computed at four anode locations (Fig. 9) and two different mass flow rates, with the actual anode current density distribution determined from magnetic probe data. The anode surface has been linearized in these diagrams, so that in going from left to right one progresses from the insulator wall at the back anode surface, around the lip, to the front face. The favorable comparison verifies that the plasma in the vicinity of the anode is sufficiently dense and hot that the required discharge current can be passed through it to the anode without the need for local electric fields. One may even speculate that it is this match of ambient plasma conditions to the discharge current that specifies the matched mass flow for a given arc current operation, although other criteria, such as the identification of number density flow with the required arc current, may also be relevant.[6]

Anode Current Conduction at Underfed Conditions

Regrettably, it has not been possible to make the same comparison of anode current with electron thermal flux for the underfed condition, $\dot{m} = 1.2$ g/sec. In this case the electrostatic and magnetic probe data in the vicinity of the anode are exceedingly noisy and irreproducible, and it is therefore impossible to define characteristic values of the plasma properties and current densities over most of the anode surface other than to identify the sizable electric field extending far from the anode surface, and the greater extension of the current pattern over the surface region (Fig. 9a). In the absence of better data at the anode, the following hypothesis is advanced: at this low mass flow the electron number density near the anode is lower than that demanded by the random flux condition invoked above, presumably because of the lower over-all density level in the chamber. Hence, in order to satisfy the current demands at the anode, the arc establishes an anode field whose function is to increase the electron flux at the anode to the proper level, and the arc current spreads itself over a larger portion of the anode surface to alleviate somewhat the local demand for electron flux density.

It may be instructive to distinguish two means by which this anode region electric field may function to accomplish the needed increase in electron flux to the anode surface: a) local resistive heating of the plasma to increase the ionization level and/or the electron temperature to the point where the random flux of electrons again becomes adequate; b) electron conduction in the prevailing field to compensate for the deficiency of random electron flux at this low density situation. Two elementary calculations estimate the relative effectiveness of these two mechanisms.

Let $(\Delta j_e)_R$ and $(\Delta j_e)_C$ define the increases in electron flux to the anode produced by resistive heating of the plasma and by electron conduction, respectively, where

$$(\Delta j_e)_R = (\partial j_e/\partial n_e)\Delta n_e + (\partial j_e/\partial T_e)\Delta T_e \tag{8}$$

$$(\Delta j_e)_C = (\partial j_e/\partial u_e)\Delta u_e \tag{9}$$

and u_e denotes the electron drift velocity in the prevailing field. The relative importance of the two terms in the expression for $(\Delta j_e)_R$ depends strongly on the state of the plasma under consideration. For example, if the plasma is only partially ionized, further energy input will increase the degree of ionization with the electron temperature changing only slightly until full ionization is approached. If the plasma is almost completely ionized,

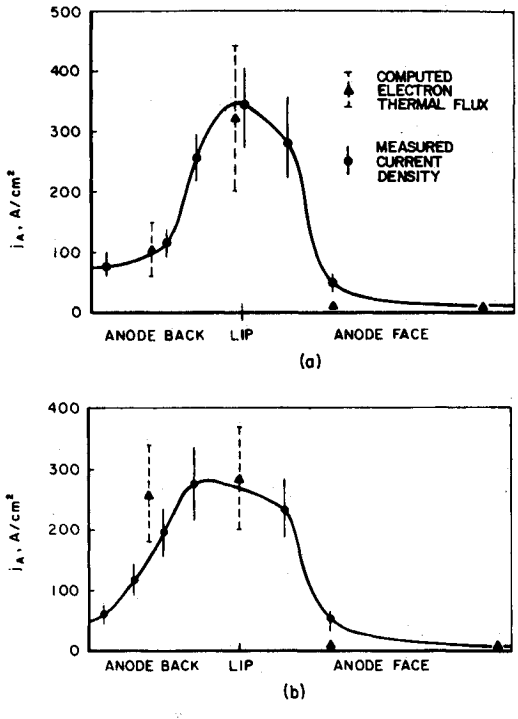

Fig. 10 Computed electron random flux compared to measured current density at anode surface at 17.5 ka: a) $\dot{m}$ = 5.9 g/sec; b) $\dot{m}$ = 36 g/sec.

on the other hand, the energy addition will first be reflected by an increase in the electron temperature rather than by the onset of substantial second ionization because of the high-energy threshold of the latter process. Unfortunately, few data are presently available on the ionization levels in the anode region of the quasi-steady MPD discharge. However, measurements of electron temperature near the anode indicate that T_e does not increase in response to anode field development at underfed mass flows and, hence, the second term on the right of Eq. (8) will be neglected.

The remaining derivatives can be evaluated from elementary kinetic theory[11]

$$\partial j_e/\partial n_e \approx (ec_e/4)\exp[-(m_e u_e^2/2kT_e)] \tag{10}$$

$$\partial j_e/\partial u_e \approx n_e(e/2)\{1+2\,\mathrm{erf}[(m_e u_e^2/2kT_e)^{1/2}]\} \tag{11}$$

Since u_e is much smaller than c_e or $(kT_e/m_e)^{1/2}$, the ratio of the two increments in anode current can be written

$$(\Delta j_e)_R/(\Delta j_e)_C \approx (2kT_e/\pi m_e)^{1/2}(\Delta n_e/\Delta u_e n_e) \approx \Delta\bar{n}_e/2\Delta\bar{u}_e \tag{12}$$

where $\Delta\bar{n}_e$ denotes the fractional increment in electron density and $\Delta\bar{u}_e$ is the increment in electron drift velocity perpendicular to the anode normalized by the electron mean thermal velocity.

The respective increases in electron number density and electron drift velocity, Δn_e and Δu_e, must now be related to the field increase at the anode, ΔE_a, by means of suitable ionization and conduction models. Current conduction in the anode region of the discharge is probably tensor in nature, with the components of current parallel and perpendicular to the anode field given by $j_\parallel = \sigma E_a/(1+\Omega_e^2)$ and $j_\perp = \sigma\Omega_e E_a/(1+\Omega_e^2)$, where σ is the scalar conductivity, and Ω_e is the electron Hall parameter, of order unity. Since E_a is essentially normal to the anode surface, we may concentrate on $j_\parallel$, and the electron drift corresponding to it

$$\Delta u_e = \Delta(j_\parallel/n_e e) = \sigma E_a/(1+\Omega_e^2)n_e e \tag{13}$$

The rate of resistive heating in the anode field region plasma is j^2/σ, where j is the resultant current density, $\sigma E_a/(1+\Omega_e^2)^{1/2}$. Assuming that all of this energy goes into ionization and its immediately attendant processes, such as radiation and excitation, the rate of electron production in the anode field region may be expressed

$$dn_e/dt = (j^2/\sigma)/eV_i^* = \sigma E_a^2/(1+\Omega_e^2)eV_i^* \tag{14}$$

where V_i^* is the effective ionization potential of argon in the prevailing environment, probably about twice the atomic ionization potential.[16] To compute an ionization increment, Δn_e, we invoke a time increment, Δt_i, equal to the transit time for electron drift across the anode field region; i.e., $\Delta t_i = d_a/u_e$ where d_a is the average thickness of the anode field region. Thus the increase in electron number density at the anode due to resistive heating of the plasma becomes

$$\Delta n_e = [(j^2/\sigma)/eV_i^*]\Delta t_i = [\sigma E_a{}^2/(1+\Omega_e{}^2)eV_i^*]\, d_a/u_e \approx n_e d_a E_a/V_i^* \tag{15}$$

Substituting the expressions for Δu_e and Δn_e, given by Eqs. (13) and (15), into Eq. (12) yields the following ratio comparing the effectiveness of resistive heating and electron conduction as means of satisfying anode current demands at the underfed condition

$$(\Delta j_e)_R/(\Delta j_e)_C = (2kT_e/\pi m_e)^{1/2}\, n_e e d_a(1+\Omega_e{}^2)/\sigma V_i^* \tag{16}$$

Using the Spitzer value for σ (Ref. 17) and the numerical values, $d_a = 2$ cm, and $V_i^* = 33$ v, the ratio becomes

$$(\Delta j_e)_R/(\Delta j_e)_C \approx 1 \times 10^{-14} n_e(1+\Omega_e{}^2)/T_e \tag{17}$$

for n_e in cm^{-3} and T_e in ev.

With reference to Fig. 9a, the relative indication of current and potential contours indicate that $\Omega_e \approx 1$ at the lip region of the anode, and from twin Langmuir probe data n_e and T_e in this region are on the order of 10^{14} cm^{-3} and 1.5 ev, respectively. Thus, at the important lip region of the anode, the aforementioned ratio becomes of order unity, implying that both processes contribute significantly to the increase in anode current.

V. Summary and Conclusions

High-power, quasi-steady MPD arcs promise high specific impulse and high-efficiency plasma acceleration. Certain results of the present study speak directly to the high thermal efficiency potential of these devices. For example, an inverse dependence of anode fall voltage on local anode current density is observed for matched, quasi-steady arc operation at current levels of 8.7, 17.5, and 42.0 ka and argon mass flow rates of 1.2, 5.9, and 36.0 g/sec. Using the indicated empirical relationship, $V_a = 1.5 \times 10^3/j_a$ (v/amp/cm^2), fractional anode power loss is computed to decrease from over 50% to less than 10% as arc pulse power increases from 1–10 Mw.

The importance of mass flow rate to the satisfactory operation of the quasi-steady MPD discharge, in particular to the arc behavior in the anode region, is reaffirmed. For matched and overfed mass flows, the discharge electric fields are significant only in the major acceleration region near the cathode, and in a narrow fall region adjacent to the anode surface. Anode current conduction at these conditions is accomplished entirely by the random thermal electron flux from the adjacent arc plasma. In fact, the ability of the anode plasma to carry the requisite current by random thermal flux alone appears to bear on the specification of the matched mass flow for a given arc current.

At underfed mass flows, substantial electric fields develop around the anode in order to augment anode current conduction from the lower density plasma. Calculations indicate that these fields raise the electron flux at the anode surface both by resistive heating of the plasma, and by field-driven electron conduction. Since much of the power deposited in this anode field envelope probably is ultimately transferred to the anode surface, decreased thermal efficiencies at underfed mass flows must be anticipated. This, combined with observations of noisy arc operation and enhanced erosion, indicates a regime of operation to be avoided.

References

[1] Shih, K. T., Pfender, E., Ibele, W. E., and Eckert, E. R. G., "Experimental Anode Heat-Transfer Studies in a Coaxial Arc Configuration," *AIAA Journal*, Vol. 6, No. 8, Aug. 1968, pp. 1482–1487.

[2] Shih, K. T. and Pfender, E., "Electrode Energy Transfer Mechanics in a MPD Arc," *AIAA Journal*, Vol. 8, No. 2, Feb. 1970, pp. 211–215.

[3] Clark, K. E. and Jahn, R. G., "Quasi-Steady Plasma Acceleration," *AIAA Journal*, Vol. 8, No. 2, Feb. 1970, pp. 216–220.

[4] Ducati, A. C. and Jahn, R. G., "Repetitively-Pulsed Quasi-Steady Vacuum MPD Arc," AIAA Paper 70-167, Princeton, N.J., 1970.

[5] Clark, K. E., "Quasi-Steady Plasma Acceleration," Rept. 859, May 1969, Dept. of Aerospace and Mechanical Sciences, Princeton Univ., Princeton, N.J.

[6] Jahn, R. G., Clark, K. E., Oberth, R. C., and Turchi, P. J., "Acceleration Patterns in Quasi-Steady MPD Arcs," *AIAA Journal*, Vol. 9, No. 1, Jan. 1971, pp. 167–172.

[7] Lovberg, R. H., "Magnetic Probes," *Plasma Diagnostic Techniques*, edited by R. H. Huddlestone, and S. L. Leonard, Academic Press, New York, 1965.

[8] Chen, F. F., "Electric Probes," *Plasma Diagnostic Techniques*, edited by R. H. Huddlestone and S. L. Leonard, Academic Press, New York, 1965.

[9] Bez, W. and Höcker, K. H., "Theorie des Anodenfalls I," *Zeitschrift für Naturforschung*, Vol. 10a, 1955, pp. 714–717.

[10] Höcker, K. H. and Bez, W., "Theorie des Anodenfalls II," *Zeitschrift für Naturforschung*, Vol. 11a, 1956, pp. 118–123.

[11] Oberth, R. C., "Anode Phenomena in High-Current Discharges," Rept. 961, Dec. 1970, Dept. of Aerospace and Mechanical Sciences, Princeton Univ., Princeton, N.J.

[12] Jahn, R. G. et al., "Pulsed Electromagnetic Gas Acceleration," NASA NGL 31-001-005, Aerospace and Mechanical Sciences Rept. 634p, July 1971, Princeton Univ., Princeton, N.J.

[13] Eckert, E. R. G., "Survey on Heat Transfer at High Speeds," WADC TR 54–70, April 1954, Wright Air Development Center, Wright-Patterson Air Force Base.

[14] Jahn, R. G. et al., "Pulsed Electromagnetic Gas Acceleration," NASA NGL 31-001-005, Aerospace and Mechanical Sciences Rept., 634o, July 1970, Princeton Univ., Princeton, N.J.

[15] Turchi, P. J., "The Cathode Region of the Quasi-Steady MPD Arcjet," Dept. of Aerospace and Mechanical Sciences Rept. 940, Oct. 1970, Princeton Univ., Princeton, N.J.

[16] Cobine, J. D., *Gaseous Conductors*, Dover, New York, 1958, p. 82.

[17] Spitzer, L., Jr., *Physics of Fully Ionized Gases*, Interscience, New York, 1962, Chap. 5.